THE JOURNAL OF BIOLOGICAL CHEMISTRY VOL. 280, NO. 41, pp. 34776–34785, October 14, 2005

Reassessment of Protein Stability, DNA Binding, and Protection of *Mycobacterium smegmatis* Dps*

Received for publication, March 2, 2005, and in revised form, June 24, 2005 Published, JBC Papers in Press, July 19, 2005, DOI 10.1074/jbc.M502343200

Pierpaolo Ceci, Andrea Ilari, Elisabetta Falvo, Laura Giangiacomo, and Emilia Chiancone[1]

From the National Research Council Institute of Molecular Biology and Pathology, Department of Biochemical Sciences "A. Rossi-Fanelli," University of Rome "La Sapienza," 00185 Rome, Italy

The structure and function of *Mycobacterium smegmatis* Dps (DNA-binding proteins from starved cells) and of the protein studied by Gupta and Chatterji (Gupta, S., and Chatterji, D. (2003) *J. Biol. Chem.* 278, 5235–5241), in which the C terminus that is used for binding DNA contains a histidine tag, have been characterized in parallel. The native dodecamer dissociated reversibly into dimers above pH 7.5 and below pH 6.0, with apparent pK_a values of ~7.65 and 4.75; at pH ~4.0, dimers formed monomers. Based on structural analysis, the two dissociation steps have been attributed to breakage of the salt bridges between Glu^{157} and Arg^{99} located at the 3-fold symmetry axes and to protonation of Asp^{66} hydrogen-bonded to Lys^{36} across the dimer interface, respectively. The C-terminal tag did not affect subunit dissociation, but altered DNA binding dramatically. At neutral pH, protonation of the histidine tag promoted DNA condensation, whereas in the native C terminus, compensation of negative and positive charges led to DNA binding without condensation. This different mode of interaction with DNA has important functional consequences as indicated by the failure of the native protein to protect DNA from DNase-mediated cleavage and by the efficiency of the tagged protein in doing so as a result of DNA sequestration in the condensates. Chemical protection of DNA from oxidative damage is realized by Dps proteins in a multistep iron oxidation/uptake/mineralization process. Dimers have a decreased protection efficiency due to disruption of the dodecamer internal cavity, where iron is deposited and mineralized after oxidation at the ferroxidase center.

The proteins of the Dps (DNA-binding proteins from starved cells) family are expressed by most bacteria under a variety of stress conditions to protect DNA against oxidative damage and other detrimental factors (1–3). DNA protection is achieved by a dual action. DNA binding itself provides an effective physical shield against damaging molecules, whereas the highly conserved ferroxidase center affords chemical protection under oxidative stress conditions in particular. Chemical protection is achieved in a multistep process that has been characterized in *Escherichia coli* Dps, the family prototype (4). In the first step, Fe(II) is bound at the ferroxidase center, where it is oxidized most efficiently by hydrogen peroxide, thus avoiding hydroxyl radical production through Fenton chemistry. In the subsequent uptake/mineralization steps, Fe(III) is sequestered as a ferric core inside the protein cavity, wherefrom it can be released upon reduction (5).

All Dps proteins are endowed with ferroxidase activity, but not all of them are capable of binding DNA, although the family was named after this property. In *E. coli* Dps, interaction with DNA involves the freely mobile, lysine-rich N termini that extend beyond the four-helix bundle of each subunit and protrude from the dodecamer surface toward solvent (6, 7). Accordingly, the inability to interact with DNA correlates either with an N terminus of reduced length, as in *Listeria innocua* Dps, *Bacillus anthracis* Dlp-1 and Dlp-2, and *Helicobacter pylori* neutrophil-activating protein (8–10), or with its immobilization on the protein surface, as in *Agrobacterium tumefaciens* Dps (11).

A recent *in vitro* work on *E. coli* Dps revealed the occurrence of two different modes of DNA binding that depend on the number of positive charges carried by the N terminus (7). The native protein, in which the intact N terminus contains 1 arginine and 3 lysines, promotes DNA condensation with formation of large Dps-DNA complexes, a situation reminiscent of the rapid formation of Dps-DNA co-crystals in starved *E. coli* cells that overexpress Dps (12). In contrast, the DpsΔ18 deletion mutant, in which the N terminus lacks all positively charged amino acids, binds DNA very weakly without causing condensation. The same study also demonstrated that DNA condensation is coupled tightly to Dps self-aggregation, a phenomenon that takes place in the absence of DNA. Thus, at physiological pH values in low ionic strength buffers (30–50 mM), native *E. coli* Dps condenses DNA and has a strong tendency to self-aggregate and precipitate out of solution. Conversely, the DpsΔ18 deletion mutant, which is unable to condense DNA, has no tendency to self-aggregate.

In this framework, *Mycobacterium smegmatis* Dps represents a most interesting model system. It is characterized by a truncated, uncharged N terminus and by a freely mobile, 26-amino acid long C-terminal extension (13) that contains both positively and negatively charged amino acid side chains (3 lysines and 2 arginines plus 1 aspartic acid and 3 glutamic acids) and, in principle, could substitute the N terminus in the interaction with DNA. Indeed, Gupta and Chatterji (14) reported recently that *M. smegmatis* Dps forms large complexes with DNA. However, these authors cloned and purified a C-terminally tagged protein containing the KPAAALEHHHHHH sequence precisely in the region responsible for the interaction with DNA. The same authors also observed that the tagged protein undergoes dissociation into trimers at low temperature (4 °C). In other Dps proteins, the dodecamer assemblage is extremely stable, *e.g.* in *L. innocua*, Dps dissociation takes place below pH 2.0 and gives rise to dimers (15). The difference in the nature of the dissociation product is of functional relevance. Trimer formation would entail loss of ferroxidase activity due to disruption of the ferroxidase center, which has an unusual location at the dimer interface, with both symmetry-related subunits providing the iron ligands (8).

* This work was supported by grants from the Ministero Istruzione Università e Ricerca "Biologia Strutturale e Dinamica di Proteine Redox," the Centro di Eccellenza Biologia e Medicina Molecolare, and Fondo Investiment Ricerca di Base 2001 (to E. C.). The costs of publication of this article were defrayed in part by the payment of page charges. This article must therefore be hereby marked "*advertisement*" in accordance with 18 U.S.C. Section 1734 solely to indicate this fact.

The atomic coordinates and structure factors (code 1UVH) have been deposited in the Protein Data Bank, Research Collaboratory for Structural Bioinformatics, Rutgers University, New Brunswick, NJ (http://www.rcsb.org/).

[1] To whom correspondence should be addressed: Istituto di Biologia e Patologia Molecolari CNR, Dipartimento di Scienze Biochimiche, Università di Roma "La Sapienza," P. le A. Moro, 5, 00185 Roma, Italy. Tel.: 39-6-494-0543/39-6-4991-0761; Fax: 39-6-444-0062; E-mail: emilia.chiancone@uniroma1.it.

In this study, the subunit dissociation, DNA binding, and protection properties of native, untagged *M. smegmatis* Dps (DpsMs)[2] were assessed in parallel with those of the tagged protein (DpsMs-His) to establish possible differences between the two proteins ascribable to the C-terminal tag. Untagged and tagged dodecamers dissociated into dimers in a similar fashion. At variance with subunit dissociation, DNA binding was affected dramatically by the tag. Thus, unlike the tagged protein, the native one was unable to promote DNA condensation, a phenomenon attributed to compensation of positive and negative charges within the C-terminal extension. Accordingly, the tagged protein protected DNA from DNase-mediated cleavage, whereas the native protein afforded no protection. Notably, dimers protected DNA from oxidative damage to a lesser extent than did dodecamers. In turn, this difference proves that iron mineralization inside the protein cavity contributes significantly to the chemical protection activity of Dps proteins by effectively removing iron from solution.

The *M. smegmatis* Dps system is of interest not only for understanding the strategies employed by Dps proteins to regulate the interaction with DNA, but also because this rapidly growing mycobacterium was recognized recently as a human pathogen usually associated with soft tissue or wound infections, a source of pulmonary infections in susceptible people following trauma and healthcare-associated procedures (16, 17). Moreover, DpsMs has 82.5% similarity and 75.6% identity to Dps from *Mycobacterium avium* ssp. *paratuberculosis*, a facultative intracellular bacterium known to cause paratuberculosis, a chronic, progressive disease, mainly in ruminants (18). *M. avium* has been invoked also as a possible a causative agent of some cases of inflammatory bowel disease in humans, especially Crohn disease (19).

MATERIALS AND METHODS

Construction of DpsMs—The *dps* gene was amplified by PCR from the *M. smegmatis* MC2 genome using primers Myc1 (5′-AAGGAGCA-CATATGACCTCATTCACCATCCC-3′) and Myc2 (5′-GTTCTA-AGCTTGGCAGACTTGCGGCGCGCC-3′). The restriction sites for NdeI and HindIII are underlined. The amplified fragment (570 bp) was digested with NdeI and HindIII, purified using the QIAquick PCR purification kit (Qiagen Inc.), and cloned into the expression vector pET-22b (Novagen) digested with NdeI and HindIII. This plasmid was introduced into *E. coli* BL21(DE3) and sequenced by dideoxy sequencing to confirm the presence of the correct gene.

Construction of DpsMs-His—An *M. smegmatis* Dps protein containing 6 histidines and an additional KPAAALE sequence at the C terminus was obtained by PCR using the primers described previously (20).

Strains and Media—E. coli strain BL21(DE3) was grown at 37 °C on liquid LB medium (10 g/liter Tryptone, 5 g/liter yeast extract, and 5 g/liter NaCl) or LB plates containing 50 μg/ml ampicillin.

Expression and Purification of DpsMs—E. coli BL21(DE3) cells harboring the recombinant plasmid were grown at 37 °C in 1 liter of liquid LB medium containing ampicillin (50 μg/ml) to an absorbance of 0.6 at 600 nm. The *dps* gene was induced by addition of 0.5 mM isopropyl β-D-thiogalactopyranoside, and the culture was incubated further for 3–4 h.

Cells were harvested by centrifugation at 15,000 × *g* for 20 min; suspended in 10 ml of buffer containing 50 mM Tris-HCl (pH 7.5), 0.5 mM dithiothreitol, 1 mM EDTA, and 500 mM NaCl; and disrupted by sonication. The lysate was centrifuged at 15,000 × *g* for 45 min, and the supernatant was precipitated using two ammonium sulfate cuts at 30 and 60% (w/v) saturation. DpsMs remains in solution at 60% saturation; after centrifugation (15,000 × *g* for 45 min), the supernatant was dialyzed overnight at room temperature against 30 mM Tris-HCl (pH 7.3) and loaded onto a DEAE-cellulose column (DE52) equilibrated with the same buffer. The protein was eluted with 300 mM NaCl, purified on a Sephadex G-150 gel filtration column (Amersham Biosciences) equilibrated with 30 mM Tris-HCl and 0.15 M NaCl (pH 7.3), pooled, and stored at −75 °C. Expression and purification of DpsMs-His were performed as described for DpsMs. The purity of the preparations was probed by Coomassie Blue staining of SDS-15% polyacrylamide gels.

Protein Crystallization—Crystallization was achieved at 293 K by the hanging drop vapor diffusion technique. A 2-μl volume of the protein sample (at 7 mg/ml) equilibrated with 30 mM Tris-HCl (pH 7.5) was mixed with an equal amount of the reservoir solution containing 0.1 M HEPES-NaOH (pH 7.0–7.8) and 1.5–2.0 M $(NH_4)_2SO_4$. Crystals grew in 1 week to ~0.3 × 0.2 × 0.2 mm^3.

Data Collection and Processing—Data were collected as 1.0 oscillation frames using an MAR CCD detector on the x-ray beamline at ELETTRA (Basovizza, Trieste, Italy) at a wavelength of 1.0 Å. Data were collected at 100 K using 25% glycerol as cryoprotectant. The data analysis, performed with DENZO (21), indicated that the crystals are rombohedral (R32), with unit cell dimensions of $a = 124.3$, $b = 124.3$, and $c = 304.65$ Å. The data were scaled using SCALEPACK (21), with $R_{sym} = 0.082\%$ and $\chi^2 = 1.23$. The crystal contains four monomers/asymmetric unit, corresponding to one-third of the assembled molecule, with $V_M = 2.15$ Å^3/Da and a solvent content of ~45%.

Structure Solution and Refinement—The structure was solved by molecular replacement using, as a search probe, a truncated polyalanine model of one-third of the *E. coli* Dps dodecamer (Protein Data Bank code 1DPS). The rotational and translational searches, performed with the program AMoRE (22) in the resolution range of 10–3.0 Å, produced a clear solution corresponding to a correlation coefficient between F_c and F_o of 62.1 and to an R_F of 44.6%. Refinement of the atomic coordinates and displacement parameters was carried out by the maximum likelihood method with the program REFMAC Version 5 (23). Model building was performed using the program package XTALVIEW (24). Water molecules were added to the model manually. The final model (a tetramer) includes 624 residues (156 residues/monomer), 141 water molecules, and four iron ions with an occupancy of 0.3. The final R_{cryst} at 2.8-Å resolution is 27.2%. The quality of the model was assessed by the program PROCHECK (25). The core and allowed regions of the Ramachandran plot contain 85.2 and 14.6% non-glycine residues, respectively.

Analytical Ultracentrifugation Experiments—Sedimentation velocity experiments were carried out on a Beckman Optima XL-A analytical ultracentrifuge at 30,000 rpm and 20 °C at a protein concentration of 1 mg/ml. The buffer used was 30 mM Tris-HCl and 0.15 M NaCl at pH values ranging from 7.0 to 8.5. Because the effect of temperature on pH is large ($\Delta pH/\Delta T = -0.03$ units/°C) in this buffer system, in specific experiments, we used 30 mM MOPS and 0.15 M NaCl. The gradient of protein concentration in the cells was determined by absorption scans along the centrifugation radius at 280 nm, with three averages and a step resolution of 0.005 cm. Data were analyzed with SEDFIT (26), and the sedimentation coefficient was reduced to $s_{20,w}$ by standard procedures.

Sedimentation equilibrium experiments were performed at 12,000 or 24,000 rpm and 20 °C. The protein concentration was 1 mg/ml. DpsMs was incubated in 30 mM Tris-HCl and 0.15 M NaCl at pH 7.0 or 8.5. Data were collected at a spacing of 0.001 cm, with 10 averages in a step scan mode every 3 h. Equilibrium was checked by comparing scans up to

[2] The abbreviations used are: DpsMs, *M. smegmatis* Dps; MOPS, 3-(*N*-morpholino)propanesulfonic acid; HPLC, high performance liquid chromatography; BisTris, 2-[bis(2-hydroxyethyl)amino]-2-(hydroxymethyl)propane-1,3-diol; dsDNA, double-stranded DNA; AFM, atomic force microscopy.

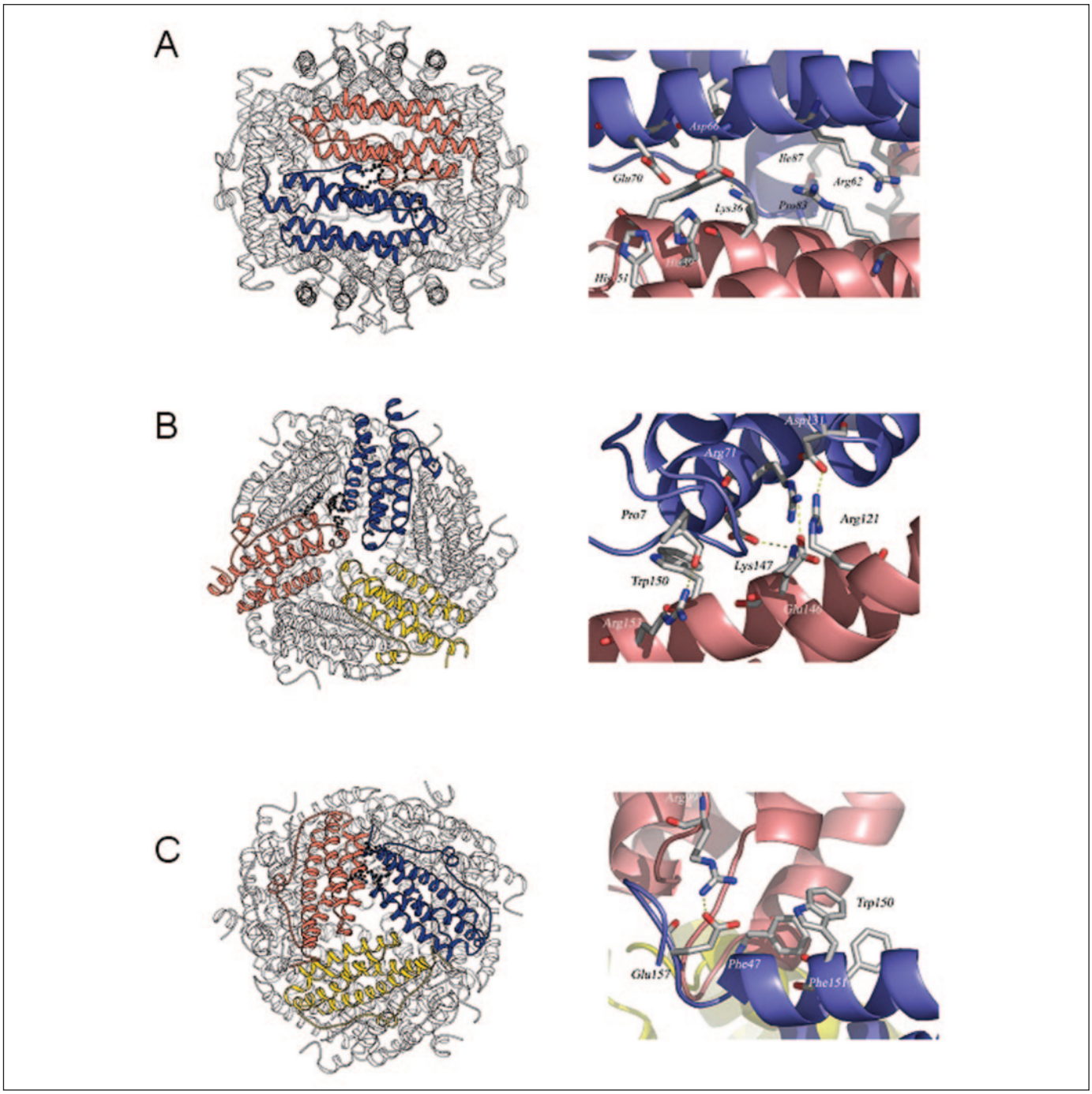

FIGURE 1. **View along the dimer (*A*), ferritin-like (*B*), and Dps-like (*C*) interfaces in DpsMs.** The *right panels* show enlargements of the interfaces indicating relevant residues involved in salt bridge formation and hydrophobic and hydrophilic interactions as detailed under "Results." The view in *A* is from the internal cavity. The images were generated using PYMOL (33) and MOLSCRIPT (34).

24 h. Data sets were edited with REEDIT (35) and fitted with WINNONLIN (36).

HPLC and Gel Filtration Experiments—DpsMs (50 μl) was applied to a TSKgel G3000SW XL 7.8/30 column (Tosoh Bioscience, Inc.) on an Amersham Biosciences HPLC system and was eluted at pH 3.0–7.4 at a flow rate of 0.8 ml/min at 25 °C. The buffers used were 100 mM glycine HCl, 100 mM acetic acid-sodium acetate, 100 mM BisTris-HCl, and 100 mM Tris-HCl, all in the presence of 0.15 M NaCl. DpsMs was used 1, 5, and 10 mg/ml. Horse spleen ferritin (450 kDa), *E. coli* Dps (221 kDa), ovalbumin (43 kDa), and myoglobin (16.9 kDa) were run independently under the same conditions to calibrate the column. The operating conditions and specifications for the TSKgel G3000SW XL column do not permit analyses below pH 7.4. For experiments at higher pH values, gel filtration chromatography was performed on a Superdex 75 column (Amersham Biosciences) in 100 mM Tris-HCl and 0.15 M NaCl (pH 7.7) at 25 °C or a Sephadex G-150 column in 30 mM Tris-HCl and 0.15 M NaCl (pH 7.6) at 25 °C. In particular, the Superdex 75 column was used to investigate the kinetic aspects of the association-dissociation processes.

Circular Dichroism Spectroscopy—CD measurements were performed at 20 °C using a Jasco J-710 spectropolarimeter. Near-UV spectra (250–310 nm) were recorded using 0.1-cm optical path quartz cells (Hellma). The protein concentration was 4 mg/ml in 30 mM Tris-HCl

TABLE ONE

Hydrophilic interactions stabilizing the dimer and trimer interfaces in *M. smegmatis*, *L. innocua*, and *E. coli* Dps proteins

M. smegmatis Dps		*L. innocua* Dps		*E. coli* Dps	
	Å		*Å*		*Å*
Dimer interface					
Lys^{36} N-ζ–Asp^{66} O-δ1	2.0–2.5	Trp^{32} N-ε1–Asp^{58} O-δ1	2.5–2.8	Lys^{48} N-ζ–Asp^{78} O-δ2	2.8–3.0
Lys^{36} N-ζ–Asp^{66} O-δ2	2.8–3.0			Arg^{70} N-η2–Asp^{78} O-δ2	2.9–3.2
Arg^{90} N-2–Gly^{84} O	3.1–3.2				
Ferritin-like interface					
Lys^{147} N-ζ–Glu^{70} O-ε2	2.4–2.8	Lys^{141} N-ζ–Glu^{62} O-ε1	2.9–3.0	Arg^{18} N-ε–Asp^{123} O-δ1	2.7–2.9
Arg^{71} N-η1–Glu^{146} O-ε2	2.4–2.5	Lys^{114} N-ζ–Glu^{126} O-δ2	2.5–2.7	Arg^{83} N-η1–Asp^{156} O-δ1	2.8–2.9
Arg^{121} N-η2–Asp^{131} O-δ1	2.4–2.5	Arg^{63} N-η2–Asp^{140} O-δ1	2.9–3.0	Arg^{133} N-η1–Asp^{20} O-δ1	2.8–2.9
				Lys^{134} N-ζ–Asp^{20} O-δ2	2.9–3.0
Dps-like interface					
Asn^{46} N-δ2–Pro^{45} O	2.5–3.2	His^{37} N-δ1–Asn^{38} O-δ1	3.2–3.4		
Arg^{99} N-η1–Glu^{157} O-ε2	2.3–2.8	Asp^{96} O-δ2–His^{37} N-ε2	3.2–3.3		

and 0.15 M NaCl at pH 7.0 or 8.5. Spectra were taken by averaging eight accumulations.

Gel Retardation Assay—The DNA binding ability of DpsMs and DpsMs-His was assessed in gel shift assays using supercoiled pUC9-5S (3115 bp, 20 nM) or a 500-bp double-stranded DNA (dsDNA) fragment as a probe. DNA was purified using the QIAprep spin plasmid miniprep kit or the QIAquick gel extraction kit (Qiagen Inc.) to ensure removal of impurities and salts. DNA was incubated for 15 min at room temperature with the Dps proteins (3 μM) in 30 mM Tris-HCl and 50 mM NaCl at pH 7.0, 7.4, or 8.0. To resolve the Dps-DNA complexes, electrophoresis was carried out on 1% agarose gels in the same buffer used for incubation of the Dps/DNA mixture. The gels were stained with ethidium bromide or Coomassie Blue and imaged using ImageMaster VDS (Amersham Biosciences). The pUC9-5S plasmid preparation used is characterized by multiple bands that can be ascribed to catenated intermediates in plasmid replication apparent in atomic force microscopy (AFM) measurements (data not shown). Moreover, only one band was present on the gels after digestion of the plasmid with HindIII.

DNA Protection from DNase—DNA protection from DNase I-mediated cleavage was assayed *in vitro* using pUC9-5S (3115 bp, 20 nM) as a probe. DpsMs and DpsMs-His (2 μM) were incubated with DNA at 25 °C in 30 mM Tris-HCl, 50 mM NaCl, 5 mM and $NiSO_4$ (pH 7.0) for 5 min and thereafter with 0.3 unit of DNase I for 5 min. The reactions were stopped by incubation with 2% SDS at 85 °C for 5 min. The reaction mixtures were loaded onto 1% agarose gel in Tris acetate/EDTA.

DNA Protection from Oxidative Damage—DNA protection from oxidative damage was assessed *in vitro* using pUC9-5S (20 nM). The dissociated and undissociated forms of DpsMs were separated by gel filtration chromatography on a Sephadex G-150 column equilibrated with 30 mM Tris-HCl and 0.15 M NaCl (pH 7.6). The damage assay was carried out in a 15-μl volume of 30 mM Tris-HCl and 0.15 M NaCl (pH 7.6). Plasmid DNA was allowed to interact with the DpsMs proteins (2 μM) for 10 min prior to addition of 50 μM $FeSO_4$. After 2 min, H_2O_2 was added at a final concentration of 10 mM, and the mixtures were incubated for 3 min at room temperature to allow complete consumption of Fe(II) (3). Thereafter, 2% SDS was added to the reaction mixture, which was incubated at 85 °C for 5 min. Plasmid DNA was resolved by electrophoresis on 1% agarose gel in Tris acetate/EDTA. The gel was stained with ethidium bromide and imaged using ImageMaster VDS.

AFM—Dps-DNA complexes were prepared by incubating the protein (50 nM) with DNA (2 nM) at 20 °C for 5 min in 50 mM Tris-HCl (pH 7.0) containing 2 mM $NiCl_2$. Sample deposition onto freshly cleaved ruby mica (Mica, New York) and AFM measurements were performed as described by Ceci *et al.* (7).

RESULTS

Structure Solution and Refinement—The *M. smegmatis* Dps protein containing the KPAAALEHHHHHH tag at the C terminus was crystallized in the hexagonal space group (R32). The structure was solved at 2.8-Å resolution by molecular replacement using *E. coli* Dps (Protein Data Bank code 1DPS) as a search probe and deposited in the Protein Data Bank (code 1UVH). The model contains 157 residues; the first 4 and the last 22 residues plus the C-terminal tag are not visible, an indication that these residues are freely mobile just as the N terminus in *E. coli* Dps (6). Only slight differences (limited to the N and C termini) are apparent with respect to the structures obtained by Roy *et al.* (13) for the same protein crystallized in the $P6_3$, $P4_32_12$, and F432 space groups. Native DpsMs did not form crystals under the conditions used to crystallize the tagged protein or under those covered by the Crystal Screen crystallization kit (Hampton Research Corp., Aliso Viejo, CA).

The DpsMs dodecamer shares the architecture of all known Dps proteins (6, 9, 10, 11, 27): identical subunits, folded into a four-helix bundle, form a hollow shell (~90 Å in diameter) characterized by tetrahedral 23 symmetry. The symmetry of the molecule leads to two nonequivalent environments along the 3-fold axes: one is typical of Dps proteins, whereas the other resembles the environment along the 3-fold axes of canonical ferritins with octahedral 432 symmetry, hence the respective names "Dps-like" and "ferritin-like" interfaces.

Like all Dps proteins, DpsMs has a ferroxidase center at the interface of 2-fold symmetry-related subunits. It contains one iron atom coordinated by Asp^{66} and Glu^{70} of one subunit and by His^{39} of the symmetry-related subunit; the site occupancy is 0.33. Iron is bound also in the cubic crystal form of Roy *et al.* (13) with a 0.4 site occupancy.

Analysis of the Dodecamer Interfaces—Although analysis of the 2-fold and 3-fold interfaces in terms of solvent-accessible surface was performed by Roy *et al.* (13), the specific interactions that stabilize the various interfaces were not detailed. This information is relevant to understanding the structural basis of the subunit dissociation process. Therefore, the analysis was repeated using a 1.4-Å radius probe, and the residues involved in intersubunit interactions were identified using the AREAIMOL program (CCP4 package) (16). For comparative purposes, the *E. coli* and *L. innocua* Dps proteins were analyzed in parallel.

The surface area buried upon dimerization, 1290 $Å^2$/monomer, is similar to those calculated with the same probe for *E. coli* and *L. innocua*

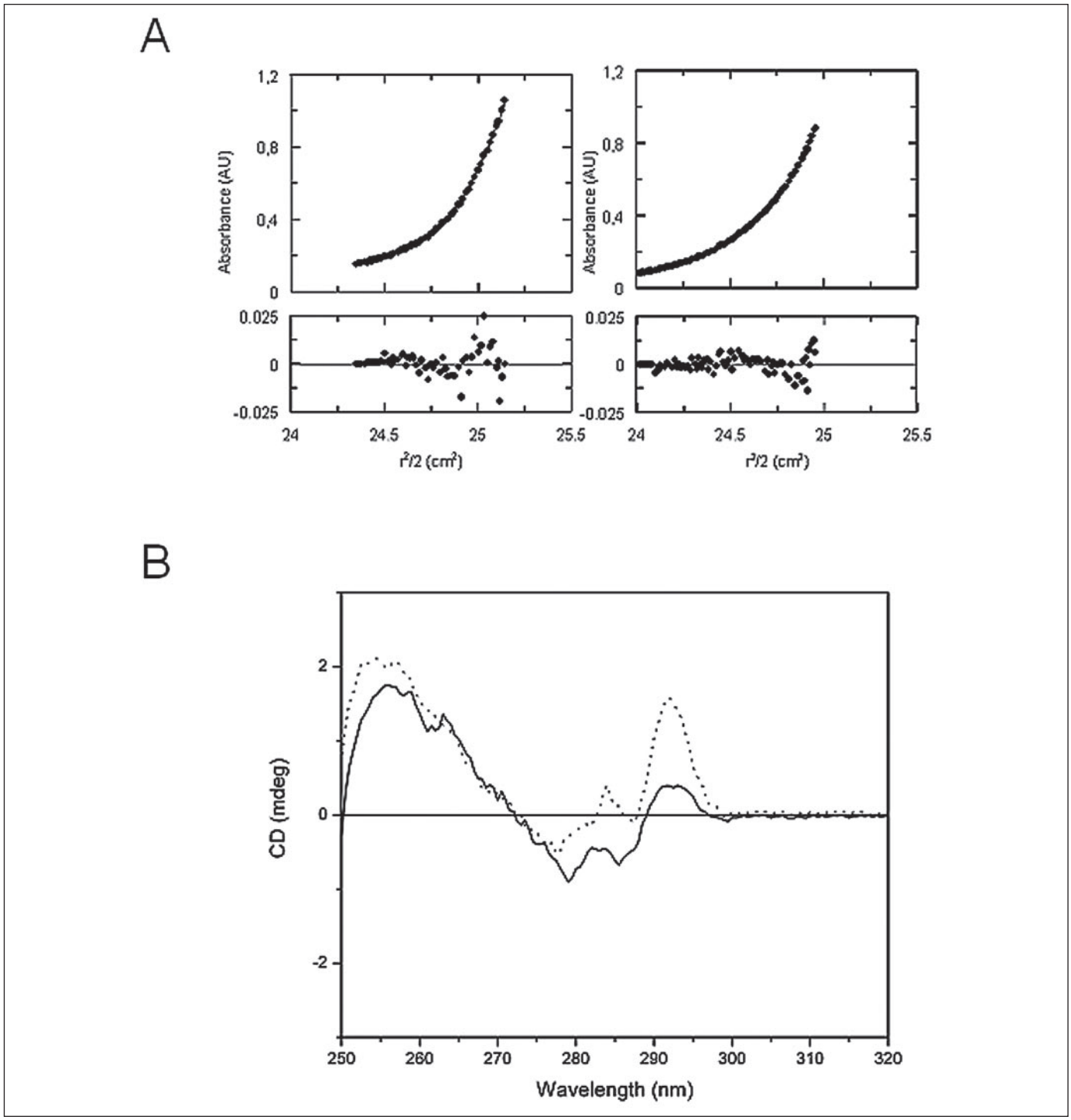

FIGURE 2. **Sedimentation equilibrium (*A*) and near-UV CD spectra (*B*) of DpsMs dodecamers and dimers.** *A*, the experiments were conducted at pH 7.0 and 12,000 rpm (*left panel*) and at pH 8.5 and 24,000 rpm (*right panel*) at a concentration of 1 mg/ml in 30 mM Tris-HCl and 0.15 M NaCl. The data were fitted to a single species with a molecular mass of 230 ± 10 kDa (*left panel*) and 41 ± 2 kDa (*right panel*); residuals are shown in the *lower panels*. *AU*, absorbance units. *B*, the protein concentration was 4 mg/ml in 30 mM Tris-HCl and 0.15 M NaCl. ····, dodecamers at pH 7.0; ——, dimers at pH 8.5. *mdeg*, millidegrees.

Dps, 1540 and 1205 Å^2/monomer, respectively. The dimer interface is formed by helices A and B and by the short BC helix placed in the middle of the long loop connecting helices B and C (Fig. 1*A*). As in other Dps proteins, the buried residues are mostly hydrophobic: Leu^{33} and Trp^{40} (helix A), Ala^{69} and Ala^{73} (helix B), and Ile^{87} and Pro^{83} (helix BC). However, in DpsMs, the dimer interface is stabilized also by two strong salt bridges formed between Lys^{36} (N-ζ) and Asp^{66} (O-δ2) of the 2-fold symmetry-related subunits (Fig. 1*A* and TABLE ONE).

Along the ferritin-like interfaces, the surface of the mycobacterial protein is lined by negatively charged residues, *viz.* Asp^{131}, Glu^{146}, and Asp^{136}. The buried surface area is extended (1397 Å^2/monomer) and involves mostly the CD loop and the beginning of helix D (Fig. 1*B*). Both hydrophobic and hydrophilic interactions stabilize the interface. The most buried hydrophobic residues are Trp^{150}, and Ile^{139} (helix D), Leu^{132} (CD loop), and Val^{77} (helix B). The interface is stabilized also by three salt bridges: one between O-δ1 of Asp^{131} (CD loop of one subunit)

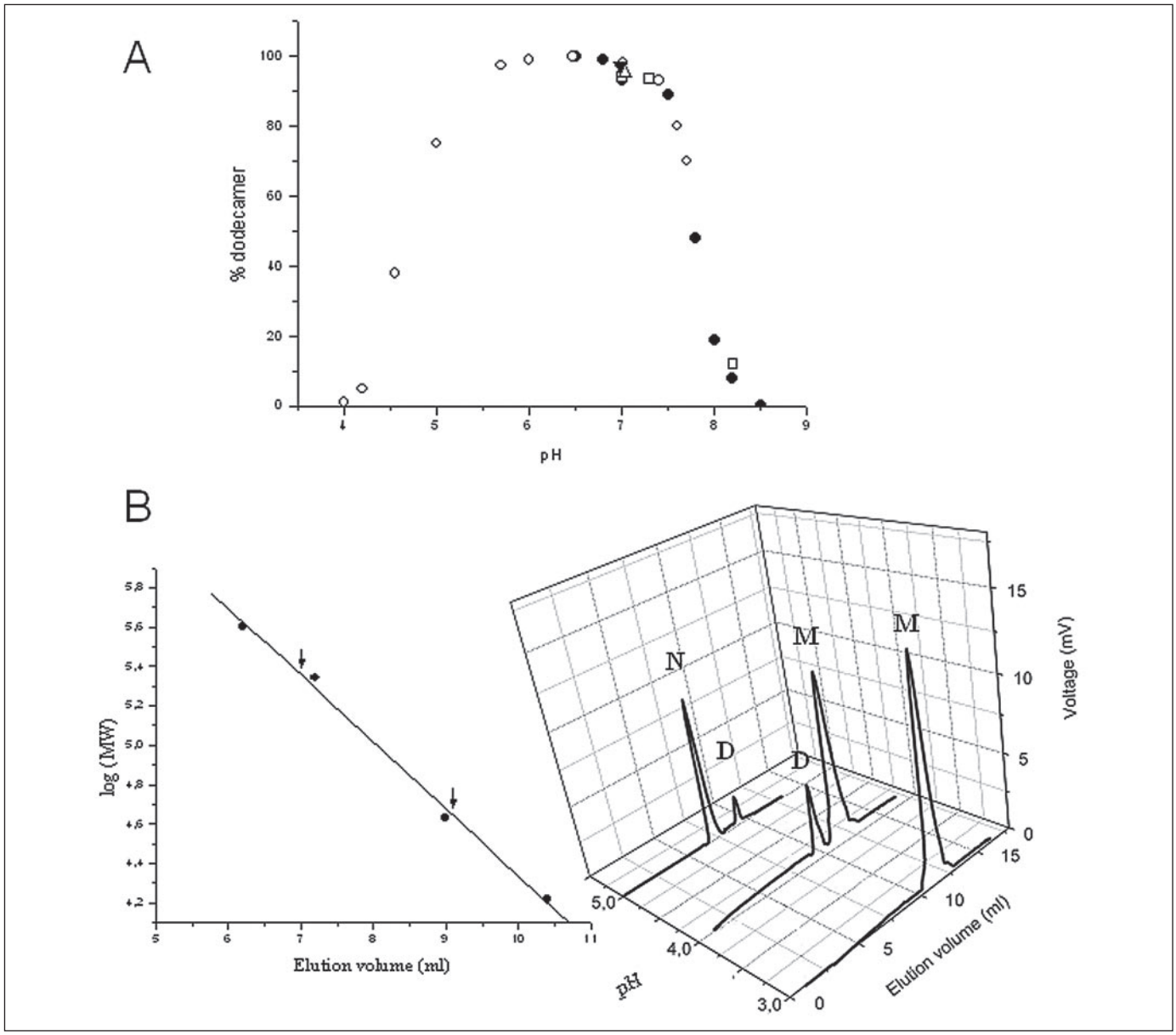

FIGURE 3. **State of association of native and C-terminally tagged DpsMs as a function of pH.** *A*, DpsMs (○ and ●) and DpsMs-His (□) were analyzed by analytical ultracentrifugation (● and □) and HPLC/gel filtration (○). The reversibility of dissociation was tested after dialysis of DpsMs solutions at pH 8.2 (▼) or 4.5 (△) against pH 7.0 buffer. *B*, DpsMs incubated at 25 °C at pH 5.0, 4.0, and 3.0 was analyzed by gel filtration. The peaks in the *right panel* correspond to the dodecameric (*N*), dimeric (*D*), and monomeric (*M*) species. The *left panel* shows the calibration curve of the TSKgel G3000SW XL column; the elution volumes of dodecameric and dimeric DpsMs are indicated by *arrows*.

and N-η2 of Arg^{121} (helix C of the 3-fold symmetry-related subunit); the second between O-ϵ2 of Glu^{146} (helix D of one subunit) and N-η2 of Arg^{71} (helix B of the symmetry-related subunit); and the third between Lys^{147} and Glu^{70} placed at the end of helices D and B, respectively (Fig. 1*B* and TABLE ONE). These salt bridges are present also in *E. coli* and *L. innocua* Dps; in the latter protein, Arg^{121} is replaced with Lys^{114}.

The Dps-like interface is formed by residues 154–159 and by the ends of helix A and of the BC loop (see Fig. 3*A*). The buried surface area (934 Å^2/monomer) is significantly smaller than in the dimer and ferritin-like interfaces. The stabilizing interactions are mostly hydrophilic; among these are a strong salt bridge between Arg^{99} of one subunit and Glu^{157} on the C-terminal end of the symmetry-related one (N-η1–O-ϵ2 distance of 2.29 Å) and two hydrogen bonds: one between N-δ2 of Asn^{46} on helix B of one subunit and the main chain oxygen of Pro^{45} and the other between the main chain N-η of Gly^{44} and the main chain oxygen of Ala^{154} (Fig. 1*C* and Table I). In *L. innocua* and *E. coli* Dps, this interface is mainly hydrophobic, and the Arg^{99}–Glu^{157} salt bridge is lacking.

State of Association—The state of association of DpsMs and DpsMs-His was analyzed as a function of pH and temperature to establish the molecular mass of the dissociation products and possible differences in the stability of the protein ascribable to the His tag. Sedimentation velocity experiments carried out at 20 °C showed that, at pH 7.0 and 8.5, only the undissociated protein or its dissociation products were present, respectively. Thus, at pH 7.0, DpsMs sediments as a homogeneous peak of 9.9 S, which corresponds to a molecular mass of ~210 kDa, assuming a spherical shape and a partial specific volume of 0.736 ml/g (28). In contrast, at pH 8.5, the sedimentation velocity is 3.1 S, which corresponds to a molecular mass of ~37 kDa, suggestive of dissociation of dodecamers into dimers based on the same assumptions. (The molecular masses for dimers and dodecamers calculated from the amino acid composition are 40.5 and 243.2 kDa, respectively.) Sedimentation equi-

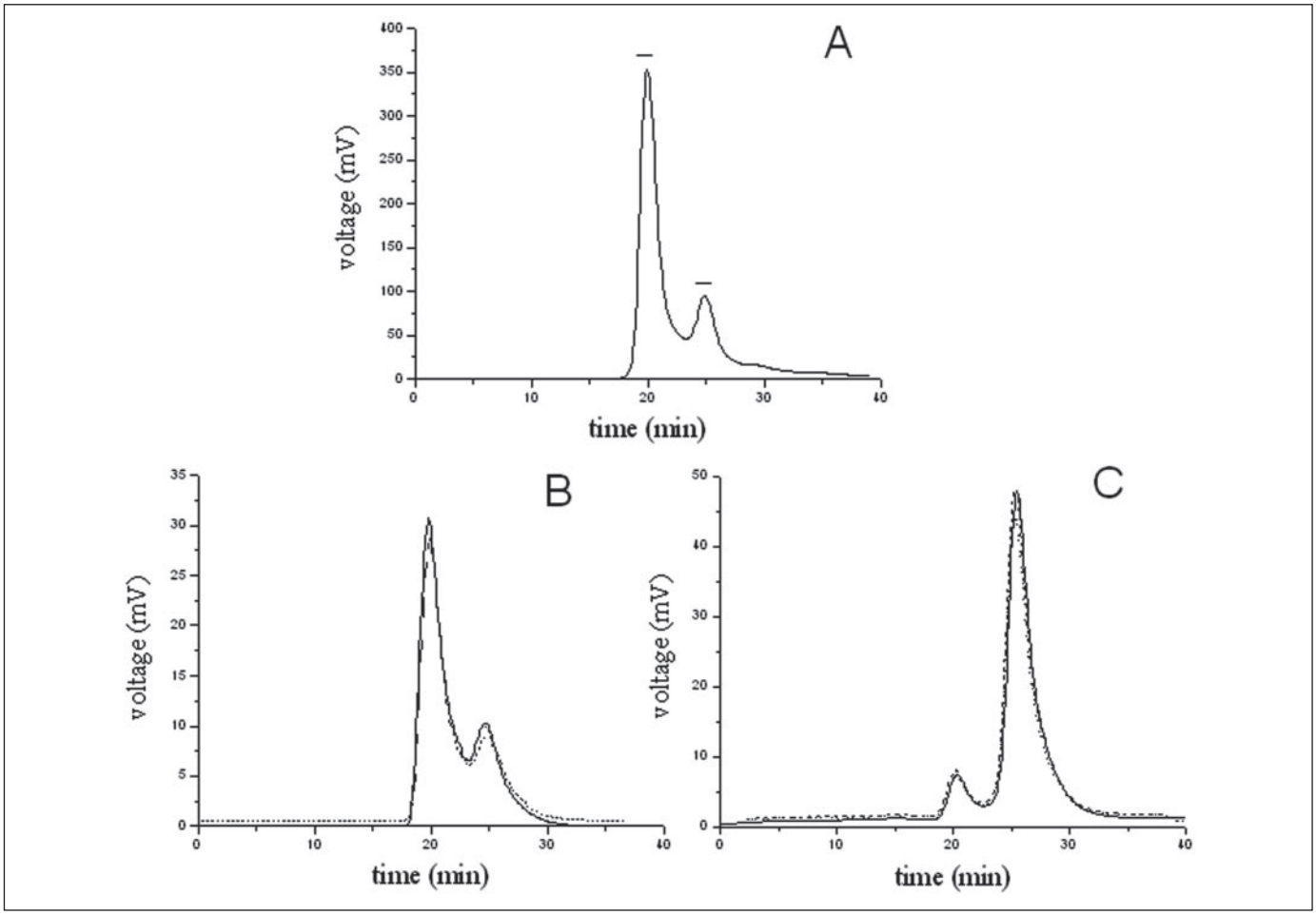

FIGURE 4. **Behavior of partially dissociated DpsMs as a function of time.** *A*, gel filtration elution pattern of DpsMs at pH 7.7 and 25 °C. The dimer (25 min) and dodecamer (20 min) fractions that were collected and analyzed subsequently are indicated. *B* and *C*, analysis of the dodecamer and dimer fractions as a function of time: 40 min (——), 180 min (– – –), and 2 days (- - - -). For details, "Results."

librium was used to determine unequivocally the molecular masses of the two stable forms of the protein. DpsMs solutions at pH 7.0 and 8.5 were analyzed in the same run at 12,000 and 24,000 rpm. At both pH values, the data fit to a single species (Fig. 2*A*). The molecular masses of 230 ± 10 and 41 ± 2 kDa correspond to dodecamers and dimers, respectively, in full agreement with the sedimentation velocity data.

The pH dependence of dissociation was studied in the alkaline and acid pH range. In sedimentation velocity experiments, dissociation became apparent at pH ~7.4 and increased sharply with increasing pH such that the transition was complete at pH ~8.5 (Fig. 3*A*). HPLC/gel filtration yielded similar results. In 100 mM Tris-HCl and 0.15 M NaCl (pH 7.0), DpsMs eluted as a single peak at ~244 kDa, the dodecamer mass, whereas at pH 7.4, a minor additional peak appeared with an elution volume corresponding to ~42 kDa, the dimer mass (Fig. 3*B*). The same results were obtained upon decreasing the NaCl concentration in the buffer from 0.15 to 0.015 M (data not shown).

Protein stability in the acid pH range was studied solely by HPLC/gel filtration (see Figs. 5 and 6). The region near the isoelectric point, *i.e.* pH ~5.5, could not be investigated because DpsMs precipitates. Dissociation into dimers was apparent upon incubation at pH 5.0; it was characterized by a very sharp pH dependence such that dodecamers were no longer visible at pH 4.0. At this pH value, dissociation proceeded beyond the dimer stage, with formation of monomers (~80%). At pH 3.0, only monomers were observed.

Notably, DpsMs and DpsMs-His are characterized by the same pH dependence of the state of association (Fig. 3*A*). This similarity confirms the indication of the x-ray structures that the C terminus is freely mobile and does not establish significant interactions with the surface of the molecule. Furthermore, both the alkaline and acid dissociation of the DpsMs dodecamer are reversible. Thus, dialysis of solutions at pH 8.2 or 4.5 against pH 7.0 buffers resulted in full reassociation of the dissociated protein into dodecamers (Fig. 3*A*). A last important feature of the subunit dissociation process is that dimers could be separated from dodecamers by gel filtration under conditions of partial dissociation of the dodecamer, *e.g.* at pH 7.6. This enabled determination of the DNA protection ability of both oligomeric forms (see below).

The kinetic aspects of the association-dissociation processes of DpsMs were investigated in HPLC/gel filtration experiments on a Superdex 75 column in 100 mM Tris-HCl and 0.15 M NaCl (pH 7.7) at 25 °C. Relevant fractions of the dimeric and dodecameric forms were collected (Fig. 4*A*), stored at 25 °C in a thermostatted cell, and reloaded onto the column as a function of time. As shown in Fig. 4 (*B* and *C*), the dodecamer fraction dissociated to the same extent as the original solution within 45 min, whereas the dimer fraction reassociated only slightly, with no significant changes up to 2 days.

Gupta and Chatterji (14) reported the occurrence of dodecamer dissociation in Tris buffer at 4 °C. Because the pH variation as a function of temperature is large in this buffer system, DpsMs was exposed to low

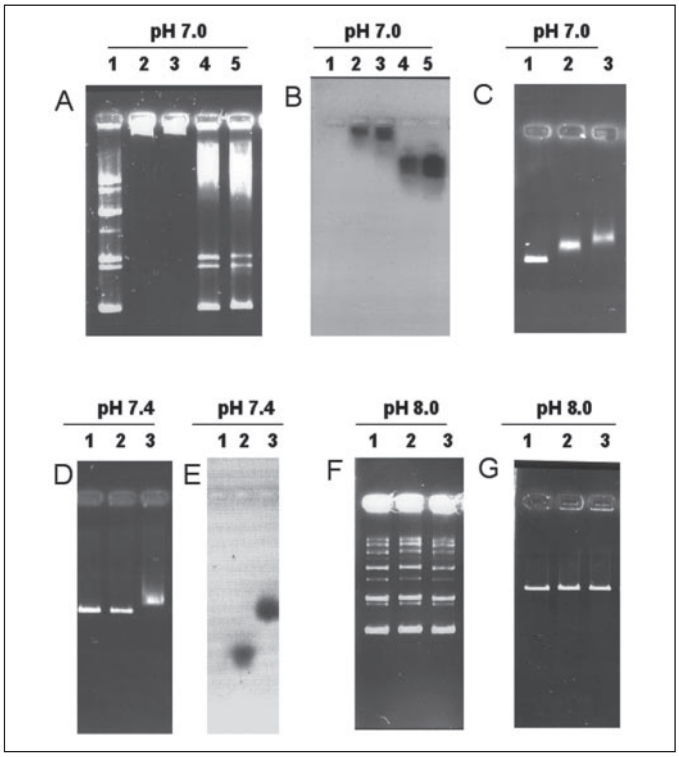

FIGURE 5. **Comparison of the interaction of native and C-terminally tagged DpsMs with DNA at different pH values assessed by DNA gel retardation assays.** *A* and *B*, 20 nM plasmid DNA alone (*lane 1*) or with 1 and 3 μM dodecameric DpsMs-His (*lanes 2* and *3*, respectively) or dodecameric DpsMs (*lanes 4* and *5*, respectively); *C*, 20 nM linear 500-bp dsDNA alone (*lane 1*) or with 1 and 3 μM dodecameric DpsMs (*lanes 2* and *3*, respectively); *D* and *E*, 20 nM linear 500-bp dsDNA alone (*lane 1*) or with 1 μM dodecameric DpsMs or DpsMs-His (*lanes 2* and *3*, respectively); *F* (plasmid DNA) and *G* (linear 500-bp dsDNA), 20 nM DNA alone (*lane 1*) or with 1 μM dimeric DpsMs or DpsMs-His (*lanes 2* and *3*, respectively). The conditions were as follows: 30 mM Tris-HCl and 50 mM NaCl at pH 7.0 (*A–C*), pH 7.4 (*D* and *E*), or pH 8.0 (*F* and *G*); and ethidium bromide (*A*, *C*, *D*, *F*, and *G*) or Coomassie Blue (*B* and *E*) staining.

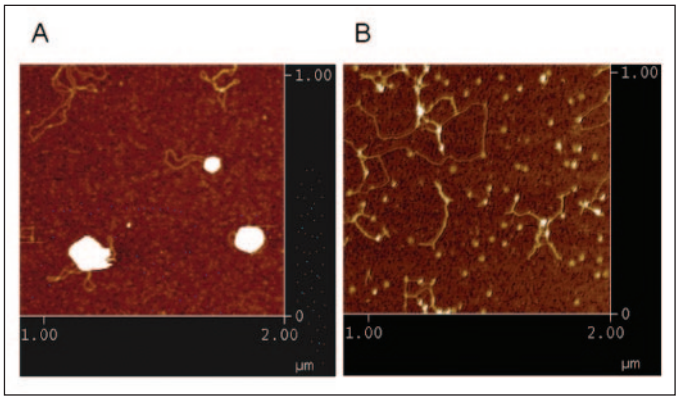

FIGURE 6. **Comparison of the interaction of native and C-terminally tagged DpsMs with DNA by AFM.** Shown are images of DpsMs-His (*A*) and DpsMs (*B*) and plasmid DNA in 50 mM Tris-HCl (pH 7.0).

temperature either in the Tris buffer used by Gupta and Chatterji or in MOPS, which is characterized by a small temperature dependence of pH. DpsMs solutions were prepared at pH 7.3 and 20 °C either in Tris buffer or in MOPS, incubated overnight at 4 °C, and analyzed by sedimentation velocity. Incubation in Tris buffer induced an increase in pH to ~7.8 and resulted in 50% dissociation into dimers, in accordance with the data of Fig. 3*A*. In contrast, no dissociation was observed upon incubation in MOPS, in accordance with the small pH variation as a function of temperature. It follows that the occurrence of dissociation

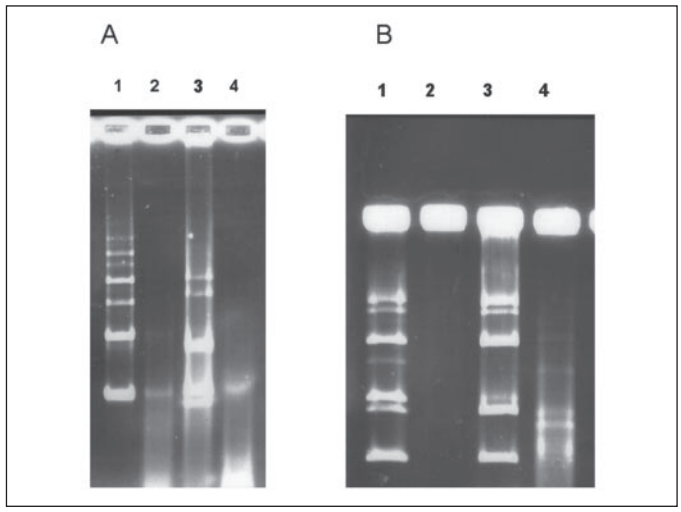

FIGURE 7. **Effect of the C-terminal tag and dimer formation assessed by *in vitro* DNA protection assays on DNase cleavage (*A*) and hydroxyl radical formation (*B*).** *A*: *lane 1*, plasmid DNA; *lane 2*, plasmid DNA exposed to 0.3 unit of DNase I; *lane 3*, plasmid DNA exposed to 0.3 unit of DNase I plus 2 μM DpsMs-His; *lane 4*, plasmid DNA exposed to 0.3 unit of DNase I plus 2 μM DpsMs. *B*: *lane 1*, plasmid DNA; *lane 2*, plasmid DNA exposed first to 50 μM $FeSO_4$ and then to 10 mM H_2O_2; *lane 3*, plasmid DNA plus 2 μM dodecameric DpsMs exposed first to 50 μM $FeSO_4$ and then to 10 mM H_2O_2; *lane 4*, plasmid DNA plus 2 μM dimeric DpsMs exposed first to 50 μM $FeSO_4$ and then to 10 mM H_2O_2.

observed by Gupta and Chatterji is not due to temperature, but to the pH change it produces in the buffer used.

Circular Dichroism Spectroscopy—Dimer formation was accompanied by a significant decrease in the ellipticity of the peaks at ~293, 283, and 281 nm attributed to vibronic transitions of tryptophan residues (Fig. 2*B*). The observed changes are in accordance with the exposure of tryptophan residues to solvent upon dodecamer dissociation because Trp^{40} is located at the dimer interface and Trp^{150} at the ferritin-like interface.

DNA Binding Assays—To compare the ability of DpsMs and DpsMs-His dodecamers and dimers to interact with DNA, agarose gel mobility shift assays were performed using supercoiled pUC9-5S DNA or a 500-bp dsDNA fragment as a probe. Reaction between Dps (1–3 μM) and DNA (20 nM) was allowed to proceed in 30 mM Tris-HCl and 50 mM NaCl.

Dodecamers were analyzed at pH 7.0. DpsMs-His generated with plasmid DNA complexes too large to migrate into the agarose gel (Fig. 5*A*, *lanes 2* and *3*), in accordance with the data of Gupta and Chatterji (14). In contrast, DpsMs dodecamers simply bound DNA as indicated by the blurring of the slowest moving band of plasmid DNA (*lanes 4* and *5*) and the marked decrease in mobility of linear dsDNA (Fig. 5*C*). Coomassie Blue staining of the gels showed that DpsMs-His precipitated and did not migrate into the agarose matrix, whereas DpsMs was fully soluble and entered the gel (Fig. 5*B*).

AFM visualization of the complexes showed that the tagged protein gave rise to large aggregates containing a large number of Dps molecules and few DNA plasmids (Fig. 6*A*), whereas DpsMs bound DNA without condensation (Fig. 6*B*), in full agreement with the gel electrophoresis results. The C-terminal tag therefore altered both the solubility of the DpsMs dodecamer at pH 7.0 and its mode of interaction with DNA. To establish whether DNA condensation can be ascribed to protonation of the histidine residues in the tag, the experiments were repeated at pH 7.4, at which histidines are significantly deprotonated. At this pH value, DpsMs-His did not self-aggregate and bound DNA with no evidence of condensation, whereas the untagged protein no longer bound DNA (Fig. 5, *D* and *E*).

Given the reversibility of the pH-induced subunit dissociation process, the ability of DpsMs and DpsMs-His dimers to interact with DNA was assayed at pH 8.0 using plasmid or a linear 500-bp dsDNA fragment as a

probe. Neither dimer affected DNA mobility (Fig. 5, *F* and *G*). The same results were obtained when the Dps concentration was increased from 1 to 5 μM while keeping the DNA concentration constant (data not shown).

DNA Protection against DNase Cleavage—To establish whether DpsMs and DpsMs-His protect DNA differently from nuclease-mediated cleavage under physiological conditions, the effect of DNase was assayed *in vitro* at pH 7.0. At this pH value, DpsMs-His condensed DNA with formation of large Dps-DNA complexes, whereas DpsMs bound DNA weakly without promoting condensation (Figs. 5 and 6). The effect of 0.3 units of DNase I on the integrity of plasmid pUC9-5S was assessed in 30 mM Tris-HCl, 50 mM NaCl, and 5 mM $NiSO_4$ in the absence and presence of the two Dps proteins. DpsMs-His afforded significant protection from DNase cleavage, whereas the extent of DNA degradation in the presence of DpsMs resembled that observed in the absence of protein (Fig. 7*A*).

DNA Protection against Hydroxyl Radical Formation—The dimeric and dodecameric forms of DpsMs were isolated by gel filtration at pH 7.6 and used immediately after separation in an *in vitro* DNA damage assay. The hydroxyl radicals formed by the combined effect of 50 μM Fe(II) and 10 mM H_2O_2 fully degraded plasmid pET-11a DNA in 30 mM Tris-HCl and 0.15 M NaCl (pH 7.6) (Fig. 7*B*, *lane 2*). Under these conditions, dodecameric DpsMs bound DNA without condensation, but afforded efficient DNA protection (*lane 3*) because it was able to carry out the complete iron oxidation/uptake/mineralization process. In contrast, dimeric DpsMs protected DNA less efficiently than the undissociated protein (*lane 4*) because iron mineralization could not take place due to destruction of the protein internal cavity. Higher pH values could not be explored because the rate of iron autoxidation became fast enough to compete with the rate of iron oxidation by hydrogen peroxide.

DISCUSSION

Mycobacterial Dps proteins are the only members of the family that employ the C terminus in the interaction with DNA. This peculiarity and the availability of a DpsMs protein tagged at the C terminus have been used to advantage to gain a deeper understanding of the structure-function relationships in Dps proteins and of the delicate charge balance that governs their mode of interaction with DNA.

As described by Roy *et al.* (13), the DpsMs dodecamer is assembled with 23 symmetry such that the N and C termini of each subunit face solvent. Accordingly, the dodecamer is stabilized mainly by interactions established by the four-helix bundles of the subunits as in all known Dps proteins. Despite this similarity, the DpsMs dodecamer is significantly less stable as a function of pH with respect to other members of the family. In the alkaline pH range, dissociation into dimers is apparent at pH ~7.6, whereas, for example, *E. coli* Dps is still undissociated at pH 8.7 (7). In the acid pH range, dissociation of DpsMs into dimers is evident at pH 5.0 and proceeds to the monomer stage at pH 4.0, at which the amount of monomers is significant. In contrast, dimer formation is apparent below pH 2.5 in *E. coli* Dps[3] and below pH 2.0 in *L. innocua* Dps, where monomers form at pH 1.0 (15).

The pH-induced dissociation depicted in Fig. 3 is a fully reversible, highly cooperative process that is not influenced by the C-terminal tag, in agreement with the flexibility of this extra extension indicated by the x-ray structure. Cooperativity, which manifests itself in the steep pH dependence of dissociation, has not been observed previously in Dps proteins, but is not unprecedented in large multisubunit assemblies (29).

The different stability of DpsMs relative to the *E. coli* and *L. innocua* proteins cannot be accounted for easily in terms of differences in the surface areas buried at the various interfaces of the dodecamer. Along the trimer interfaces that are disrupted upon dimer formation, such differences are either not significant or are in the wrong direction. Thus, as reported by Roy *et al.* (13), at the ferritin-like trimer interface, the interaction area in DpsMs is on the same order of magnitude as in *E. coli* Dps (1397 and 1419 Å^2/monomer, respectively) and significantly larger than in the very stable *L. innocua* Dps protein (870 Å^2/monomer). The surface area buried at the Dps-like trimer interface has the same order of magnitude in these proteins (934, 971, and 802 Å^2/monomer in *M. smegmatis*, *E. coli*, and *L. innocua* Dps, respectively).

It follows that specific interactions stabilizing the interfaces have to be invoked. The ferritin-like trimer interface is mostly hydrophilic and contains three salt bridges in DpsMs that are conserved in *E. coli* and *L. innocua* Dps. In contrast, the Dps-like trimer interface, characterized by the smallest buried surface area, differs in nature in DpsMs and in the *E. coli* and *Listeria* proteins. In DpsMs, it contains charged residues accounting for 25% of the buried area and a strong salt bridge between Glu^{157} and Arg^{99} (TABLE ONE). In *E. coli* and *L. innocua* Dps, Arg^{99} is not conserved, and the interface is stabilized mostly by hydrophobic patches formed by Phe, Ile, and Trp residues. (The charged residues occupy 12–14% of the buried surface.) Based on this analysis, disruption of the unique salt bridge between Glu^{157} O-ϵ2 and Arg^{99} N-η1 could account for dissociation of the DpsMs dodecamer in both the acid and alkaline pH range. The 2 residues are buried in a hydrophobic milieu; and, in addition, N-η2 of Arg^{99} is hydrogen-bonded to the main chain oxygen of Gly^{76} (distance of 2.6 Å) of the 2-fold symmetry-related subunit. Therefore, their pK_a values are expected to be altered with respect to water (30). In particular, the pK_a of the Glu^{157} side chain could be raised to ~4.75, and conversely, the pK_a of Arg^{99} could be depressed to ~7.65, corresponding to the pK values of acid and alkaline dissociation. This assignment, which will need mutagenesis studies for confirmation, requires in turn that the pH dependence of dissociation into dimers be the same in the acid and alkaline pH range, as was indeed observed (Fig. 3).

Analysis of the dimer interface provides information on the dimer-monomer dissociation step. In the three Dps proteins considered, the buried surface area is similar (1290, 1540, and 1205 Å^2/monomer for *M. smegmatis*, *E. coli*, and *L. innocua* Dps, respectively), and the relevant residues are mostly hydrophobic. However, the interface of DpsMs has two features that account for its decreased stability relative to the interface of the *Listeria* protein. The hydrophobic interactions between the helices B and C are weaker in DpsMs than in *L. innocua* Dps because Pro^{83} and Ile^{87} substitute for 2 leucines (Leu^{55} and Leu^{79}). In addition, the DpsMs interface contains two salt bridges between Lys^{36} and Asp^{66} of the symmetry-related subunits, whereas strong hydrophilic interactions are lacking in *L. innocua* Dps (15). The dimer-monomer dissociation step that occurs with an apparent pK of ~3.6 can be ascribed to disruption of these interactions attendant upon protonation of Asp^{66}.

The C-terminal tag affected the mode of interaction with DNA, but did not influence the dissociation process of DpsMs. The effect was dramatic under physiological conditions, *e.g.* at pH 7.0, at which the tagged protein gave rise to DNA condensates, and DpsMs bound DNA without condensation, and also at pH 7.4, at which the tagged protein bound DNA, and the native protein was no longer able to do so (Fig. 5, *A–D*). As observed for *E. coli* Dps, DNA condensation by DpsMs-His was linked tightly to self-aggregation of the protein in the absence of DNA. In *E. coli* Dps, these two processes take place provided the N terminus contains at least one protonated lysine side chain, as indicated by the behavior of deletion mutant DpsΔ8 (7). In DpsMs-His, the two processes took place at pH 7.4, but not at pH 7.0 and are therefore most likely due to protonation of the histidine residues in the tag (Fig. 5*D*, *lane 3*). Interestingly, native DpsMs was unable to self-aggregate and to pro-

[3] P. Ceci, A. Ilari, E. Falvo, L. Giangiacomo, and E. Chiancone, unpublished data.

mote DNA condensation despite the presence of 3 lysines and 2 arginines in the long, flexible C terminus. It follows that their positive charge must be compensated by the four negative charges carried by the C-terminal carboxylate residues. The use of charge compensation within the DNA-binding region as a means to regulate Dps self-aggregation and the mode of DNA binding has not been reported before. It is reminiscent of the use of single charged side chains to avoid edge-to-edge aggregation of designed β-strands (31).

The different interaction of the tagged and untagged proteins with DNA is of functional relevance. Thus, DpsMs-His was able to protect DNA efficiently from DNase-mediated cleavage, consistent with the sequestration of DNA in the condensates. No such protection was afforded by DpsMs, which, although interacting with DNA, was unable to cover the DNA backbone fully (Figs. 6 and 7). The difference in protection efficiency between the tagged and untagged proteins was not apparent in the hydroxyl radical-mediated DNA degradation experiments. In this case, DNA does not need to be occupied by protein because efficient scavenging of any incoming Fe(II) can be achieved even if the Fe(II) binding activity is localized in the vicinity of DNA.

The possibility of studying isolated Dps dimers provided by the present system is of value in this regard, as it provides a means to distinguish the specific contributions of the ferroxidation and mineralization steps in affording chemical protection to DNA. DpsMs dimers are already set up to protect DNA due to the presence of the ferroxidase center. However, the absence of an internal cavity that permits effective removal of iron from solution results in a significant decrease in the protection efficiency relative to the native protein. To our knowledge, this is the first experimental proof of the importance of the iron sequestration step. The DNA binding ability of the dimeric forms of DpsMs and DpsMs-His could not be assessed because, at the pH values at dimers are stable, no interaction with DNA can be expected to occur given the strong pH dependence of the DNA binding-condensation processes (Fig. 5, *F* and *G*). Notably, at the pH values (6.1–7.2) occurring in the DpsMs cytoplasm (32), Dps is a stable dodecamer endowed with efficient DNA protection capacity against free radical damage that can contribute to survival of the bacterium.

In conclusion, the present reassessment of the DpsMs properties adds to our understanding of several structural features that have functional ramifications in Dps proteins. Protonation/deprotonation of a specific salt bridge at the Dps-like interface can modulate the stability of the dodecamer as a function of pH, and charge compensation within the DpsMs C terminus determines the occurrence of self-aggregation and the nature of the Dps-DNA interaction product, yet additional proof of the delicate charge balance that regulates these phenomena. The dodecamer assemblage is required for efficient chemical protection of DNA because it provides a nanocage structure for iron mineralization, whereas protection from DNase-mediated cleavage depends on sequestration of DNA in Dps-DNA condensates.

Acknowledgments—We thank Dr. Giovanni Dehò for providing M. smegmatis DNA and Drs. Sara Cellai and Claudio Rivetti for carrying out the AFM experiments.

REFERENCES

1. Nair, S., and Finkel, S.E. (2004) *J. Bacteriol.* **186,** 4192–4198
2. Yamamoto, Y., Poole, L. B., Higuchi, M., and Kamio, Y. (2000) *J. Bacteriol.*, **182,** 3740–3747
3. Pulliainen, A. T., Haataja, S., Kahkonen, S., and Finne, J. (2003) *J. Biol. Chem.* **278,** 7996–8005
4. Zhao, G., Ceci, P., Ilari, A., Giangiacomo, L., Laue, T. M., Chiancone, E., and Chasteen, N. D. (2002) *J. Biol. Chem.* **277,** 27689–27696
5. Ilari, A., Ceci, P., Ferrari, D., Rossi, G. L., and Chiancone, E. (2002) *J. Biol. Chem.* **277,** 37619–37623
6. Grant, R. A., Filman, D. J., Finkel, S. E., Kolter, R., and Hogle, J. M. (1998) *Nat. Struct. Biol.* **5,** 294–303
7. Ceci, P., Cellai, S., Falvo, E., Rivetti, C., Rossi, G. L., and Chiancone, E. (2004) *Nucleic Acid Res.* **32,** 5935–5944
8. Bozzi, M., Mignogna, G., Stefanini, S., Barra, D., Longhi, C., Valenti, P., and Chiancone, E. (1997) *J. Biol. Chem.* **272,** 3259–3265
9. Papinutto, E., Dundon, W. G., Pitulis, N., Battistutta, R., Montecucco, C., and Zanotti, G. (2002) *J. Biol. Chem.* **277,** 15093–15098
10. Zanotti, G., Papinutto, E., Dundon, W. G., Battistutta, R., Seveso, M., Del Giudice, G., Rappuoli, R., and Montecucco, C. (2002) *J. Mol. Biol.* **323,** 125–130
11. Ceci, P., Ilari, A., Falvo, E., and Chiancone, E. (2003) *J. Biol. Chem.* **278,** 20319–20326
12. Wolf, S. G., Frenkiel, D., Arad, T., Finkel, S. E., Kolter, R., and Minsky, A. (1999) *Nature* **400,** 83–85
13. Roy, S., Gupta, S., Das, S., Sekar, K., Chatterji, D., and Vijayan, M. (2004) *J. Mol. Biol.* **339,** 1103–1113
14. Gupta, S., and Chatterji, D. (2003) *J. Biol. Chem.* **278,** 5235–5241
15. Chiaraluce, R., Consalvi, V., Cavallo, S., Ilari, A., Stefanini, S., and Chiancone, E. (2000) *Eur. J. Biochem.* **267,** 5733–5741
16. Ergan, B., Coplu, L., Alp, A., and Artvinli, M. (2004) *Respirology* **9,** 283–285
17. Skiest, D. J, and Levi, M. E. (1998) *South. Med. J.* **91,** 36–37
18. Whittington, R. J., Marshall, D. J., Nicholls, P. J., Marsh, I. B., and Reddacliff, L. A. (2004) *Appl. Environ. Microbiol.* **70,** 2989–3004
19. Chacon, O., Bermudez, L. E., and Barletta, R. G. (2004) *Annu. Rev. Microbiol.* **13,** 329–363
20. Gupta, S., Pandit, S. B., Srinivasan, N., and Chatterji, D. (2002) *Protein Eng.* **15,** 503–512
21. Ottwinowski, Z., and Minor, W. (1997) *Methods Enzymol.* **276,** 307–326
22. Navaza, J. (1994) *Acta Crystallogr. Sect. A* **50,** 157–163
23. Murshudov, G. N., Lebedev, A., Vagin, A., Wilson, K. S., and Dodson, E. J. (1999) *Acta Crystallogr. Sect. D* **55,** 247–255
24. McRee, D. E. (1993) *Practical Protein Crystallography*, pp. 365–374, Academic Press, Inc., Orlando, FL
25. Laskowski, R. A., McArthur, M. W., Moss, D. S., and Thornton, J. M. (1993) *J. Appl. Crystallogr.* **26,** 283–291
26. Schuck, P. (2000) *Biophys. J.* **78,** 1606–1619
27. Ilari, A., Stefanini, S., Chiancone, E., and Tsernoglou, D. (2000) *Nat. Struct. Biol.* **7,** 38–43
28. Laue, T. M., Shah, B. D., Ridgeway, T. M., and Pelletier, S. L. (1992) in *Analytical Ultracentrifugation in Biochemistry and Polymer Science* (Harding, S. E., Rowe, A. J., and Horton, J. C., eds) pp. 90–125, Royal Society of Chemistry, Cambridge
29. Antonini, E., and Chiancone, E. (1977) *Annu. Rev. Biophys. Bioeng.* **6,** 239–271
30. Fitch, C. A., Karp, D. A., Lee, K. K., Stites, W. E., Lattman, E. E., and Garcia-Moreno, E. B. (2002) *Biophys. J.* **82,** 3289–3304
31. Richardson, J. S., and Richardson, D. C. (2002) *Proc. Natl. Acad. Sci. U. S. A.* **99,** 2754–2759
32. Rao, M., Streur, T. L., Aldwell, F. E., and Cook, G. M. (2001) *Microbiology* (*Read.*) **147,** 1017–1024
33. DeLano, W. L. (2005) *Drug Discovery Today* **10,** 213–217
34. Kraulis, P. J. (1991) *J. Appl. Crystallogr.* **24,** 946–950
35. Lary, J. W. (1998) *REEDIT*, National Analytical Ultracentrifugation Center, Storrs, CT
36. Yphantis, D. A., Johnson, M. L., and Lary, J. W. (1997) *WINNONLIN*, University of Connecticut, Storrs, CT

Reassessment of Protein Stability, DNA Binding, and Protection of *Mycobacterium smegmatis* Dps

Pierpaolo Ceci, Andrea Ilari, Elisabetta Falvo, Laura Giangiacomo and Emilia Chiancone

J. Biol. Chem. 2005, 280:34776-34785.
doi: 10.1074/jbc.M502343200 originally published online July 19, 2005
